Highly surface functionalized carbon nano-onions for bright light bioimaging

2015 Methods Appl. Fluoresc. 3 044005

(http://iopscience.iop.org/2050-6120/3/4/044005)

Methods and Applications in Fluorescence

PAPER

RECEIVED
19 May 2015

REVISED
17 August 2015

ACCEPTED FOR PUBLICATION
26 August 2015

PUBLISHED
15 October 2015

Highly surface functionalized carbon nano-onions for bright light bioimaging

Marco Frasconi[1], Viviana Maffeis[1,2], Juergen Bartelmess[1], Luis Echegoyen[3] and Silvia Giordani[1]

[1] Istituto Italiano di Tecnologia (IIT), Nano Carbon Materials Lab, Via Morego 30, 16163 Genova, Italy
[2] Department of Chemistry and Industrial Chemistry, University of Genova, Via Dodecaneso 31, 16146 Genova, Italy
[3] Department of Chemistry, University of Texas at El Paso (UTEP), El Paso, TX 79968, USA

E-mail: silvia.giordani@iit.it

Keywords: fluorescence, nanomaterials, cells, nanosensors, imaging

Abstract

Carbon-based nanomaterials functionalized with fluorescent and water-soluble groups have emerged as platforms for biological imaging because of their low toxicity and ability to be internalized by cells. The development of imaging probes based on carbon nanomaterials for biomedical studies requires the understanding of their biological response as well as the efficient and safety exposition of the nanomaterial to the cell compartment where it is designed to operate. Here, we present a fluorescent probe based on surface functionalized carbon nano-onions (CNOs) for biological imaging. The modification of CNOs by chemical oxidation of the defects on the outer shell of these carbon nanoparticles results in an extensive surface functionalization with carboxyl groups. We have obtained fluorescently labelled CNOs by a reaction involving the amide bond formation between fluoresceinamine and the carboxylic acids groups on the surface of the CNOs. The functionalized CNOs display high emission properties and dispersability in water due to the presence of high surface coverage of carboxylic acid groups that translate in an efficient fluorescent probe for *in vitro* imaging of HeLa cells, without significant cytotoxicity. The resulting nanomaterial represents a promising platform for biological imaging applications due to the high dispersability in water, its efficient internalization by cancer cells and localization in specific cell compartments.

Introduction

Carbon-based nanomaterials [1–3] have attracted enormous attention in recent years in chemistry, physics and materials science. Carbon nanomaterials (CNMs) consist of a large class of materials that includes fullerene [1], carbon nanotubes [4–6] and graphene [7, 8], as well as carbon nanohorns [9, 10], nanodiamonds (NDs) [11], multi-layer fullerenes, also known as carbon nano-onions (CNOs) [12–14], and carbon nanohoops [15–17]. One of the major drawbacks for the potential applications of CNMs is their poor solubility in common solvents. In order to improve the solubility of these nanomaterials in different solvents, surface modification of CNMs with different functional groups has been devised by either covalent or non-covalent synthetic methods [18–20]. A well-established procedure for the surface grafting of CNM is the radical addition based on the *in situ* generated diazonium salts. This methodology, firstly described for highly ordered pyrolytic graphite [21], was successfully applied for the surface functionalization of CNTs [22–24], NDs [25], graphene [26, 27] and CNOs [14, 28].

The applications of carbon nanomaterials, including graphene and its derivatives [29, 30], CNTs [31–33] as well as NDs [11, 34], in nanomedicine is well established. These nanomaterials have been widely used as theranostic delivery systems with the possibility to deliver bioactive agents and simultaneously detect selectively diseased tissues [35]. A key application of CNMs in modern biomedical research is related to their use *in vitro* and *in vivo* fluorescence imaging [36]. A rather underexplored CNM for biomedical imaging and theranostics delivery are CNOs, that are usually prepared from NDs by high-temperature thermal treatment leading to small diameter (approximately 5 nm) CNOs [13, 14, 37]. CNOs were previously applied in a variety of fields with leading examples in catalysis [38, 39], tribology [40, 41], and electronic applications such as anode materials in batteries [42, 43], in supercapacitors [44–46] and THz shielding [47]. In 2013 we published the first comprehensive analy-

sis of the inflammatory effects of CNOs functionalized with fluorescein units in both *in vivo* and *in vitro* [48]. We demonstrated that the cytotoxicity of CNOs is strongly affected by their physicochemical properties and that the inflammatory properties are controlled by the surface functionalization of the nanomaterial. In addition, we observed that the inflammatory potential of functionalized CNOs was lower than the one detected for CNTs modified with similar functional groups [48]. Indeed, current studies on cellular fate of different CNMs, including CNOs, NDs and carbon nanohorns, have demonstrated that the surface composition is critical for the *in vivo* application of these CNMs. Significant differences in the nanomaterial internalization pathway and the biological activity in cancer cells have been observed for CNO and ND constructs [36]. For example, extensive biological studies on fluorescent NDs revealed that small NDs entered human cervical cancer cells by a clathrin-mediated endocytic pathway [34]. In the present study, we have focused our attention on CNOs as highly robust, thanks to the multi-shell structure, and tunable platforms for imaging of cancer cells. In our imaging probe design, CNOs with 5 nm diameter are particularly attractive because they can be readily chemically modified on the surface. CNOs possess reactive sites that are suitable for functionalization and they offer a reasonable surface area for the attachment of a wide range of imaging, targeting and/or therapeutic agents. Fluorescently labelled CNOs have been prepared by anchoring derivatives of boron dipyrromethene on to benzoic acid groups on the CNO surface [49, 50]. The high cellular uptake of fluorescently labelled CNOs, along with their low cytotoxicity, renders these carbon based nanomaterial an ideal platform for biomedical applications. For the design of multi-functional theranostic nanomaterials, it is of great importance to develop different surface functionalization strategies. We have recently reported the functionalization of OH-terminated CNOs by a radical addition procedure [51], with a far-red/NIR emitting BODIPY derivative [52]. Another common synthetic procedure for the surface functionalization of CNOs is the oxidation of the surface with nitric acid, leading to carboxy-functionalities on the CNOs surface. These surface functionalities can be derivatized with amines [53–58]. However, none of these examples include fluorescence imaging and toxicological studies, which are fundamental for developing biomedical applications [59].

Here we report the surface functionalization of oxidized CNOs by amide coupling with fluoresceinamine. The use of fluorescein as fluorescent probe for the functionalization of CNOs is due to the high fluorescence quantum yield along with the high photostability and low toxicity of this dye [60]. Further, the ease of preparation and the availability of different functional groups, has prompted the use of this dye for the chemical functionalization of nanomaterials, including carbon based nanomaterials [36]. We have characterized the fluorescently labelled CNOs by using a variety of techniques including thermogravimetric analysis (TGA), dynamic light scattering (DLS), zeta potential as well as Fourier transform infrared (FTIR), Raman, absorption and fluorescence spectroscopies. The fluorescently functionalized CNOs have been tested as probe for *in vitro* imaging of HeLa cells. The high degree of surface functionalization together with good dispersability and low cytotoxicity of this nanomaterial will pave the way for its potential applications in biomedical imaging and for the development of novel systems for theranostic purposes.

Experimental

Material and methods

The following chemicals were purchased from Sigma-Aldrich and used as received: nitric acid, 4-dimethylaminopyridine (DMAP), *N*-hydroxysuccinimide (NHS), 1-ethyl-3-(3-dimethylaminopropyl) carbodiimide hydrochloride (EDC-HCl), fluoresceinamine (isomer I), anhydrous tetrahydrofuran (THF), dimethylformamide (DMF), dimethyl sulfoxide (DMSO), phosphate buffered saline (PBS). For cell culture study Dulbecco's modified Eagle's medium (DMEM) enriched with 10% FBS (Life Technologies), 2% Penstrep and 1% glutamine, was employed. All aqueous solutions were prepared by using deionized water, which was further purified with a Milli-Q system (Millipore) and all solvents were purchased in high purity grade. Reactions and measurements were carried out under ambient conditions, unless otherwise noted.

Synthetic procedures

p-CNO

The synthesis of small CNOs (6–8 shells) was performed by annealing nanodiamonds of 5 nm average particle size under a positive pressure of helium at 1650 °C [34].

ox-CNO

Oxidation of pristine CNOs was carried out following a modified procedure based on earlier reported methodology[50]. 40 mg of pristine CNOs were dispersed in 30 ml of a solution of nitric acid (3M) and stirred under reflux for 48 h. After cooling to room temperature, the CNOs were filtered off on a nylon filter membrane (pore size 0.2 μm) and washed with water, methanol and acetone. 38 mg of *ox*-CNO were recovered as black powder after drying over night at RT.

fluo-CNO

A dispersion of *ox*-CNO (15 mg) was prepared by ultrasonication (20 min at 37 kHz) in a mixture (30 ml) of dry THF and DMF (2 : 1). The mixture was deoxygenated under N_2 and 50 mg (0.41 mmol) of DMAP, 50 mg (0.43 mmol) of NHS and 80 mg

(0.42 mmol) of EDC-HCl were added. The reaction mixture was briefly sonicated and after the addition of 40 mg (0.12 mmol) of fluoresceinamine (isomer I) heated under reflux for 4 d under N_2. After cooling to RT, the CNOs were redispersed in DMF, filtered off (nylon membrane, pore size 0.2 μm) and washed with THF and acetone. 12 μg of *fluo*-CNO were recovered as black powder after drying under air for one day.

Instrumentation

Thermogravymetric analysis (TGA)

TGA was conducted on a TA Q500 analyser, using a Pt pan as sample holder. After equilibrating the sample at 30 °C for 5 min and then at 100 °C for additional 20 min, the measurement was performed in air using a heating rate of 10 °C/min. The sample weight was monitored until 900 °C.

Attenuated total reflectance Fourier transformed infrared (ATR FTIR) spectroscopy

The FTIR spectra were recorded with a Bruker Vertex 70v FTIR spectrometer equipped with a Platinum ATR accessory on solid samples.

Raman spectroscopy

Raman spectra were measured on a Horiba Jobin Yvon HR 800 UV LabRam Raman microscope. For the Raman measurements, the samples were excited with a built-in 632 nm laser. The samples were deposited by adding the dry compound to a drop of methanol on the glass slide. The slides were dried in air for 2 h.

Absorption and fluorescence spectroscopy

Absorption spectra were recorded on an Agilent Cary 8454 UV–vis diode array spectrophotometer. Fluorescence spectra were taken on a Horiba Jobin Yvon Fluoromax-4 spectrofluorometer in 1.00 cm × 1.00 cm quartz glass cells. The CNO samples were dispersed in DMSO, PBS 0.01M or cell medium to a final concentration of 500 μg ml^{-1}. The dispersion of CNO was sonicated for 15 min at 37 kHz and then diluted respectively in DMSO, PBS 0.01M or cell medium to achieve final concentrations of 50, 20, 10, 5 and 1 μg ml^{-1}.

Dynamic light scattering (DLS) and zeta-potential measurements

DLS Measurements were performed on the Malvern Nano-ZS instrument operating in backscattering (173°) mode and analysed with the software Zetasizer, with automatic selection of the optimal detector position and number of independent measurements. The CNO samples were dispersed in DMSO, PBS 0.01M or cell medium to a final concentration of 500 μg ml^{-1}. The samples were sonicated for 30 min at 37 kHz and then diluted respectively in DMSO, PBS 0.01M or cell medium to achieve final concentrations of 50, 20, 10, 5 and 1 μg ml^{-1}. The CNOs samples were sonicated for additional 15 min and the size of the particle was measured. Z-potential measurements were performed on the same apparatus using the disposable Z-potential cuvettes.

Confocal microscopy

Confocal imaging was performed with a laser scanning confocal microscope equipped with a resonant scanner (Nikon A1R) using a 20 × objective.

Biological methods

Sample preparation for cell study

The samples of *ox*-CNO and *fluo*-CNO were prepared by suspending 1 mg of CNOs in 1 ml sterile phosphate buffered saline (PBS) solution followed by sonication for 30 min at 37 kHz. The samples were then dispersed in the cell culture media (DMEM) at final concentrations of 1, 2, 5, 10 μg ml^{-1}.

Cell culture and viability assay

Cells were grown in monolayer culture at 37 °C under a 5% CO_2 atmosphere in a humidified environment. HeLa cells were cultured in Dulbecco's modified Eagle's medium (DMEM) enriched with 10% FBS (Life Technologies), 2% Penstrep and 1% glutamine. Cells were seeded in 24 well chamber slides at a density of 5×10^4 cells/well and incubated in a 500 μl cell culture medium to obtain a subconfluent monolayer after 48 h in a humidified atmosphere at 37 °C and 5% CO_2. The cell culture medium was removed and replaced with 500 μl of medium with dispersions of *ox*-CNO and *fluo*-CNO at the final concentrations. The viability of the cells was measured after 12, 24, 48 and 72 h of exposure to the samples of CNO, utilizing the PrestoBlue™ cell viability assay (Life Technologies). Assays were performed following a procedure previously described [61] by measuring the absorbance on a microplate reader at a wavelength of 570 nm. Each measurement was normalized with the average signal of untreated wells to determine the percent cell viability expressed as the mean ± SD.

Cellular imaging

Cells were grown in subconfluent monolayer (50–60 % confluent) on 25 mm glass bottom dishes at 37 °C under a 5% CO_2 atmosphere in a humidified environment. The culture medium was removed and replaced with 1, 5 and 10 μg ml^{-1} suspension of *fluo*-CNO and incubated for 24 h. After the incubation time, the cells were washed with PBS three times to remove any remaining media and the cells were incubated for 7 min at 37 °C with a solution of Hoechst 33342, for live nuclear staining. Excitation of the fluorescein on the CNO samples was performed at 488 nm and the emission was acquired in the spectral window between 500–560 nm. The Hoechst 33342 was exited at 405 nm and the images were acquired in the emission range of 415–480 nm.

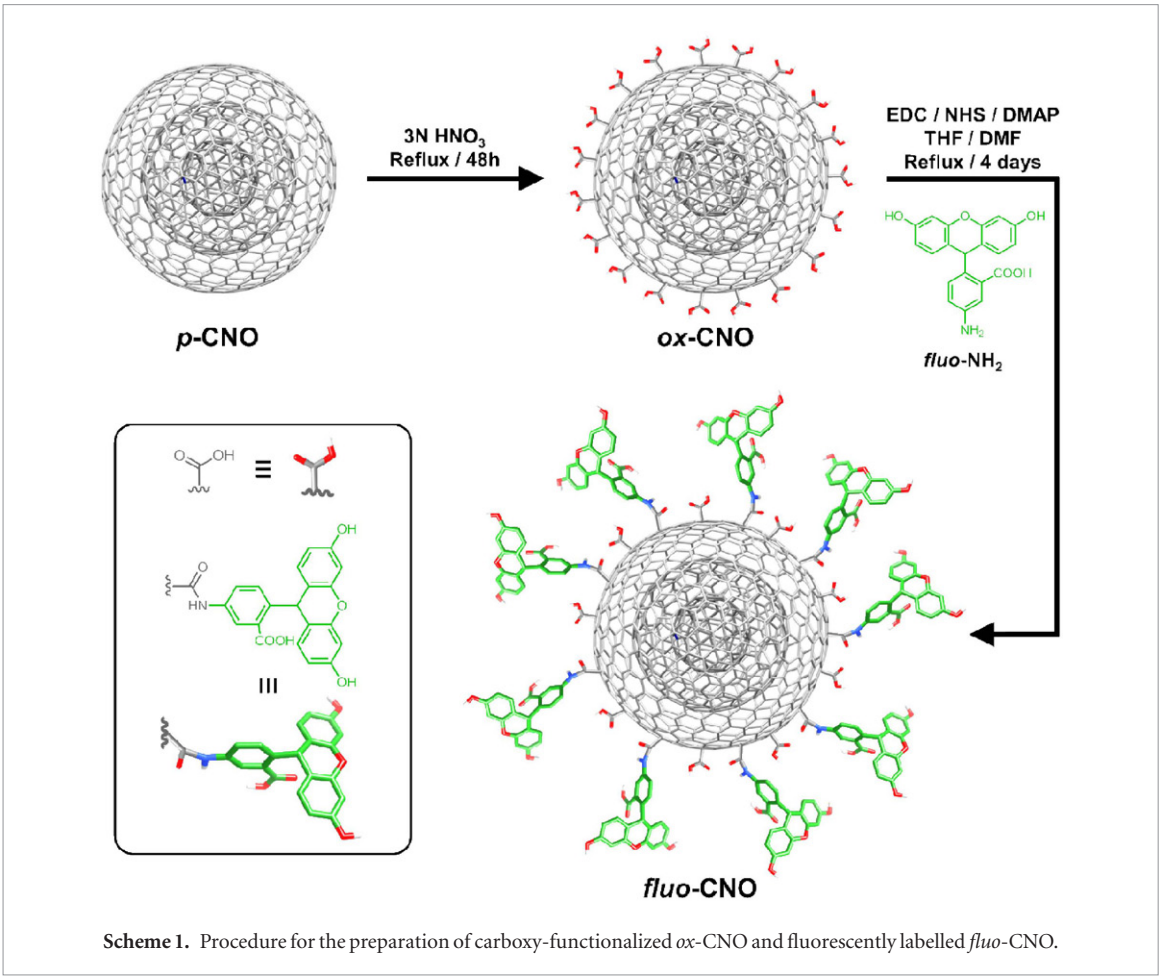

Scheme 1. Procedure for the preparation of carboxy-functionalized *ox*-CNO and fluorescently labelled *fluo*-CNO.

Results and discussion

The surface functionalization of *p*-CNO, prepared by the thermal annealing of 5 nm diameter nanodiamonds [34], was accomplished by chemical oxidation of the CNO surface to introduce carboxylic acid functional groups. The oxidation of these surface defective sites was performed by treatment of a dispersion of *p*-CNO with nitric acid (3M) under reflux conditions for 48 h (scheme 1). The resulting CNOs, named *ox*-CNO, were collected from the reaction mixture and the excess of nitric acid was removed by extensive washing with water, methanol and acetone; the *ox*-CNO sample, decorated with carboxylic acid groups, can now be dispersed in water. The attachment of the fluorescein onto the surface of the *ox*-CNO was realized by amide coupling of fluoresceinamine to the carboxylic acid groups in a mixture of THF : DMF (2 : 1), using N-hydroxysuccinimide (NHS) and 1-ethyl-3-(3-dimethylaminopropyl) carbodiimide hydrochloride (EDC-HCl), in the presence of 4-dimethylaminopyridine (DMAP) (scheme 1). After reaction, the *fluo*-CNOs were filtered-off and washed with plenty of THF and acetone in order to completely remove the fluorescein physically adsorbed on the surface of the *fluo*-CNOs. The successful surface modification of the *p*-CNO with carboxylic acid groups to yield *ox*-CNO and the coupling with fluorescein to obtain *fluo*-CNO, was corroborated by a variety of techniques. The chemical modification of *p*-CNO was confirmed by solid-state ATR FT-IR spectroscopy which displays the characteristic stretching and vibration bands of the carboxylic acid groups in the case of *ox*-CNO and the fluorescein functionalities for the *fluo*-CNOs. The FTIR spectrum of *ox*-CNO shows a peak at around 1680 cm^{-1} corresponding to the stretching vibrations of C = O (figure 1). A significant change of the FTIR spectra was observed after coupling of fluorescein amine on the surface modified CNO, and new bands corresponding to the vibrations of the fluorescein moiety are seen in the spectrum of *fluo*-CNOs. Raman spectra of *p*-CNO, *ox*-CNO and *fluo*-CNO are shown in figure 2. *ox*-CNO display a little lowering of the D-band (1320 cm^{-1}) compared to the G-band (1580 cm^{-1}), suggesting purification of the pristine CNOs from carbonaceous material upon nitric acid treatment. As expected the amidation of the carboxyl moiety leading to *fluo*-CNO did not alter significantly the ratio between the D and G bands.

The high degree of surface functionalization of the *ox*-CNOs in comparison to previously reported chemical modification of CNOs, such as the grafting of the CNO surface with benzoic acid groups by radical addition procedure, was observed by TGA analysis. TGA performed in air displays the thermal decomposition of the carboxylic acid groups, followed by the decomposition of the CNOs core. The comparison of the TGA weight loss curves (figure 3) of *p*-CNO with

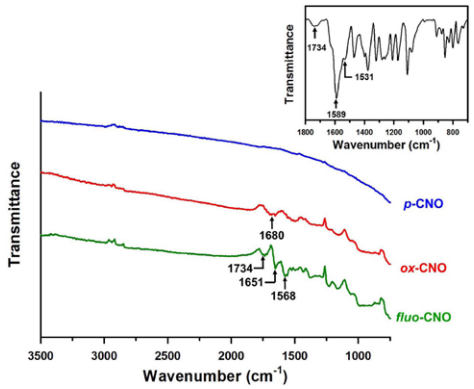

Figure 1. ATR-FTIR spectra of *p*-CNO (blue), *ox*-CNO (red) and *fluo*-CNO (green). Inset: ATR-FTIR spectra of fluoresceinamine. Each ATR-FTIR spectrum was accumulated from 256 scans with normal resolution using germanium crystals.

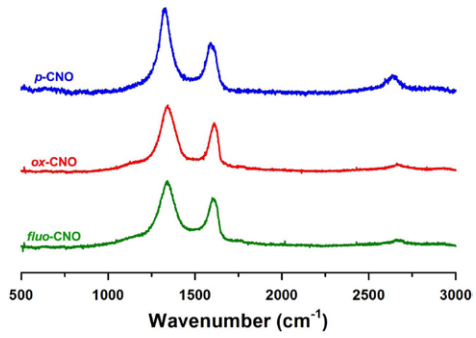

Figure 2. Raman spectra of *p*-CNO (blue), *ox*-CNO (red) and *fluo*-CNO (green). The Raman spectra were normalized for the G-band 1580 cm^{-1}.

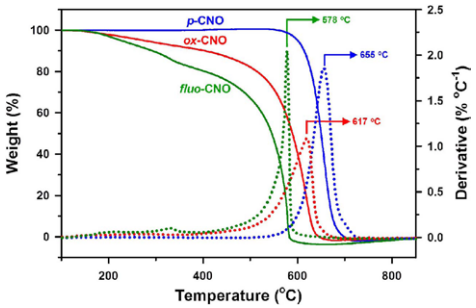

Figure 3. Thermogravimetric analysis (solid lines) and the corresponding weight loss derivatives (dotted lines) of *p*-CNO (blue), *ox*-CNO (red) and *fluo*-CNO (green). All experiments were run in air with a temperature rate of 10 °C min^{-1}.

that of *ox*-CNO reveals a decrease in the decomposition temperature from 655 to 617 °C. The coverage of carboxylic acid groups on the surface of the *ox*-CNO was calculated from the TGA weight loss at 450 °C and around 210 carboxylic functionalities per CNO were estimated. In comparison with the grafting coverage obtained from the modification of the CNOs with benzoic acid by radical addition [48–50], yielding to approximately 50 carboxylic functionalities per CNO, the modification of the CNOs by the chemical oxidation procedure described here yields a much higher grafting coverage. The attachment of fluoresceinamine on the *ox*-CNO to yield *fluo*-CNO results in a further decrease of the decomposition temperature to 578 °C, as resulted from the TGA curve. The number of fluorescein molecules per CNO was calculated form the weight loss at 450 °C of the *fluo*-CNO and are approximately 28 units per unit. A comparable degree of surface coverage of fluorescein units per CNO was obtained for different functionalization procedures reported previously [48]. On the other hand, the higher surface coverage of carboxylic acid groups obtained for the *fluo*-CNO, along with the presence of the fluorophore, results in an enhancement of the capability of the CNO constructs to be dispersable in water.

Particle dispersion and stability were systematically investigated in different conditions by dynamic light scattering (DLS) experiments. DLS measurements were performed on the CNOs samples dispersed in DMSO, phosphate buffer 0.01M or cell culture medium (DMEM with 10% FBS, 2% Penstrep and 1% glutamine). The dispersion of *ox*-CNO or *fluo*-CNO was carried out at an initial concentration of 500 μg ml^{-1} by sonication of the sample for 30 min in DMSO, phosphate buffer 0.01M (pH 7.4) or cell medium, followed by dilution of the samples to achieve final concentrations of 50, 20, 10, 5 and 1 μg ml^{-1}. Unlike previously reported CNO constructs that displayed bimodal dimensional distribution and a significant tendency to agglomerate with time, *ox*-CNO revealed an effective hydrodynamic diameter in DMSO and in phosphate buffer of 115 $\pm$ 1 nm and 105 $\pm$ 1 nm, respectively. These values of diameters does not change significantly with the time as well as the concentration of *ox*-CNO, suggesting the low tendency of these dispersions to form large agglomerates even at relatively high concentrations. Under similar conditions hydrodynamic diameters of 171 $\pm$ 8 nm and 179 $\pm$ 33 nm were measured for the *fluo*-CNO dispersed in DMSO and in phosphate buffer (table 1).

Z-potential measurements of *ox*-CNO and *fluo*-CNO samples were performed in phosphate buffer 0.01M at pH 7.4. Under these conditions the zeta-potentials for the *ox*-CNO was -41 ± 1 mV, independently on the CNO concentrations used. Only a minute change in the zeta-potential was observed after functionalization of the CNOs with fluorescein to yield *fluo*-CNO (table 1), indicating that the carboxy functionalities have a significant effect on the charging capacity of each particle. For comparison, the zeta-potential of a dispersion of *p*-CNO in phosphate buffer 0.01M was -18 ± 2 mV. DLS and zeta-potential measurements were then carried out in the cell medium in order to examine the behaviour of the CNOs under physiological conditions. The dispersion of the particles in cell medium has a dramatic effect on the behaviour of the *ox*-CNO with an average hydrodynamic diameter of 828 $\pm$ 110 nm. An average diam-

Table 1. Effective hydrodynamic diameter obtained from dynamic light scattering (DLS) measurements and zeta-potential of *ox*-CNO and *fluo*-CNO.

Sample	Effective hydrodynamic diameter (nm)			Zeta-potential (mV)	
	DMSO	PBS 0.01M	Cell medium	PBS 0.01M	Cell medium
ox-CNO	115 ± 1	105 ± 1	828 ± 110	−41 ± 1	−23 ± 1
fluo-CNO	171 ± 8	179 ± 33	225 ± 36	−38 ± 1	−20 ± 2

eter of 225 ± 36 nm was measured for a dispersion of *fluo*-CNO in cell medium. The dispersion of *ox*-CNO and *fluo*-CNO samples in cell medium resulted in a decrease of the zeta-potential values to −23 ± 1 mV and −20 ± 2 mV, respectively.

The emission properties of the fluorescein labelled CNOs were tested under different conditions. Upon photoexcitation at 490 nm of a dispersion of *fluo*-CNO in DMSO, an intense emission band was observed with a maximum at 544 nm. The fluorescence spectra of dispersions of *fluo*-CNO in phosphate buffer and cell culture medium gave rise to an emission centred at around 518 nm, which is slightly shifted in comparison to the emission of free fluorescein in PBS ($\lambda_{em} = 513$ nm). The difference in the wavelength of maximum emission between free fluorescein and *fluo*-CNO implies a different environment surrounding the fluorophores anchored on the surface of the CNOs. Another aspect relates to the photostability of the fluorescein anchored on the *fluo*-CNO. We found that a dispersion of *fluo*-CNO in phosphate buffer retains the photophysical properties upon two weeks storage at 4 °C (figure 4).

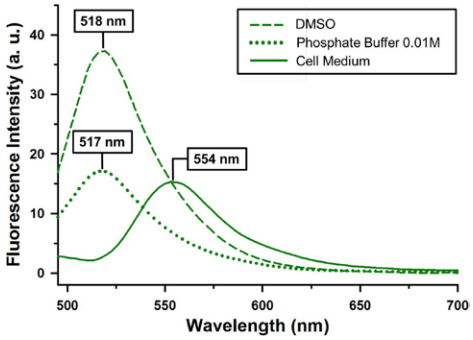

Figure 4. Emission spectra ($\lambda_{exc} = 490$ nm) of *fluo*-CNO dispersed in DMSO (solid line), phosphate buffer 0.01M (dotted line) and cell medium (dashed line). The *fluo*-CNO samples were dispersed at concentration of 10 μg ml^{-1}. The emission from the media was subtracted to the spectra of *fluo*-CNO.

The cytocompatibility of functionalized nanomaterials is a fundamental consideration when investigating their use as bioimaging agents. The cytotoxicity of *ox*-CNO and *fluo*-CNO samples dispersed in cell medium was tested at different concentrations (1, 2, 5 and 10 μg ml^{-1}) on HeLa cells. The cell viability was measured by using a resazurin-based assay and the result was expressed as percentage viability versus a control consisting of cells treated with only the cell culture medium. The obtained percentage viability at different administration time did not result in significant cytotoxicity of the differently functionalized CNOs. The viability of the HeLa cells treated with *ox*-CNO (figure 5(a)) and *fluo*-CNO (figure 5(b)) was found to be higher than 80% for an incubation time of 24 h at 37 °C at all concentrations of CNOs tested. After 48 h and 72 h of incubation, the viability of the HeLa cells treated with *ox*-CNO and *fluo*-CNO was higher than 80% for the concentrations of 1, 2 and 5 μg ml^{-1} and only at a concentration of 10 μg ml^{-1} was a decrease of cell viability to 70% observed. The low toxicity determined for the functionalized CNOs is a key requirement for the use of these fluorescent nanomaterials in biomedical applications and encourages the further investigation of these materials as imaging probes for cancer cells.

Confocal live cell imaging was performed in order to explore the ability of the fluorescein labelled CNOs to be internalized by cells and to localize their presence in cellular compartments. HeLa cells grown in subconfluent monolayer on a glass slide were treated with a dispersion of *fluo*-CNO in DMEM at concentrations of 1, 5 and 10 μg ml^{-1}. After 24 h of incubation at 37 °C, the cells were carefully rinsed with fresh media to remove the excess of CNOs and treated with Hoechst 33342, for live nuclear staining. The cellular uptake characteristics of the *fluo*-CNO in the concentration range investigated are shown in figure 6. The green fluorescence signal detected in the cells clearly indicates that *fluo*-CNOs were internalized by cells. Cells treated with 1 μg ml^{-1} *fluo*-CNO display a point-like distribution of the fluorescence signal in the perinuclear region (figure 6(a)). In agreement with previous studies on the cellular uptake of CNOs functionalized with fluorophores [49, 50], the localization of the *fluo*-CNO in living cells within the cytoplasmatic compartment is likely due to intravesicle storage of the CNOs as a consequence of the cell internalization of *fluo*-CNO by an endocytosis pathway. For higher concentrations of *fluo*-CNO, 5 and 10 μg ml^{-1} (figures 6(b) and (c)), the cells display a widely spread green emission from the fluorescein coupled onto the CNOs, indicating an efficient cellular internalization of the *fluo*-CNO.

Conclusions

We have demonstrated a versatile strategy for the preparation of highly surface modified CNOs by oxidation of the defects on the surface of CNOs and chemical functionalization of the carboxyl groups by amide coupling with fluoresceineamine. We have systematically investigated the importance of surface functionalization for the dispersion of the modified

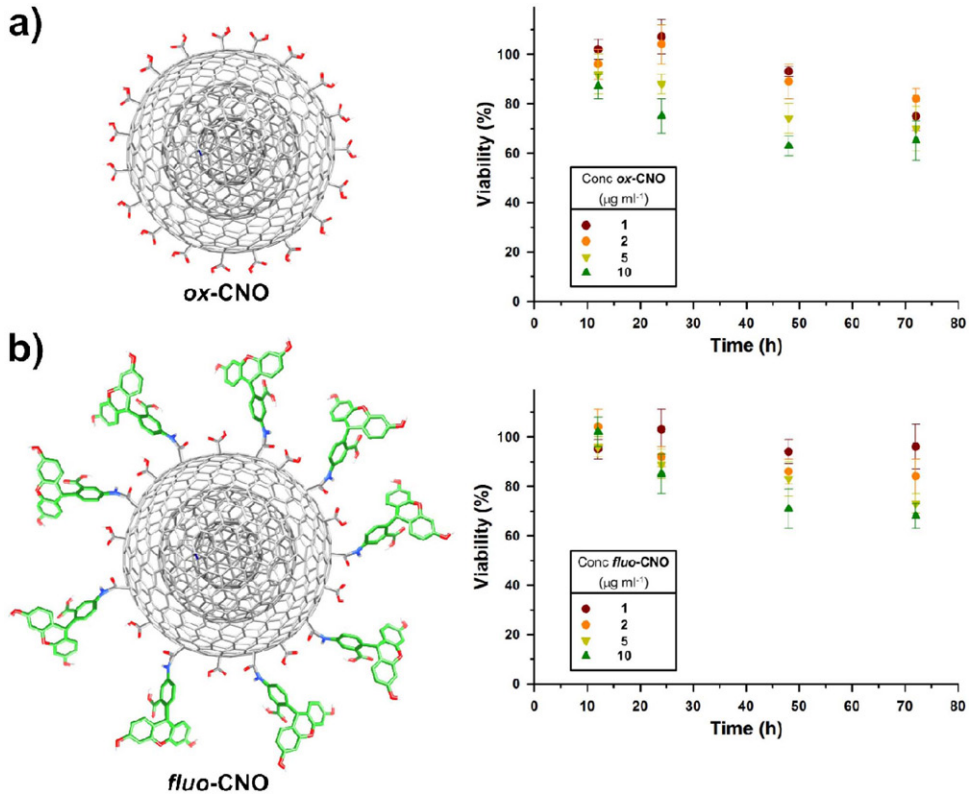

Figure 5. Cellular viability of HeLa cells after exposure to 1, 2, 5 and 10 μg ml^{-1} *ox*-CNO (a) and *fluo*-CNO (b). The viability was evaluated for the samples of CNOs against a non-treated control.

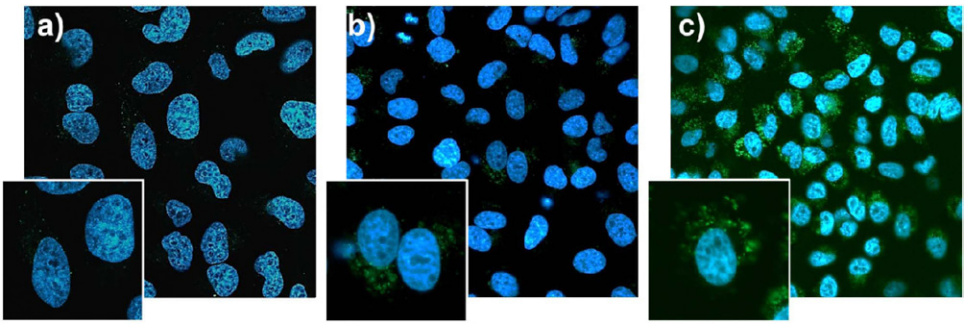

Figure 6. Confocal image of HeLa cells after incubation for 24 h with 1 (a), 5 (b), 10 (c) μg ml^{-1} of *fluo*-CNO. Cells were stained with Hoechst 33342 (blue).

CNOs in physiological conditions. The surface functionalized CNOs displays attractive properties, such as high fluorescence and dispersability in water. The high biocompatibility and minimal systemic toxicity of these fluorescent CNOs along with an efficient cellular uptake, make these functionalized CNOs suitable candidates as fluorescent probes for bioimaging studies. These highly surface functionalized carbon nanoparticles hold promise as multifunctional nanomaterial for theranostic applications.

Acknowledgments

The authors wish to thank the Istituto Italiano di Tecnologia (IIT) for funding. We are grateful to the Drug Discovery and Development, Nanophysics and Nanochemistry departments at IIT for instrumental support. We thank David Buck (UTEP) for the preparation of the pristine CNOs.

References

[1] Kroto H W, Heath J R, O'Brien S C, Curl R F and Smalley R E 1985 C60: Buckminsterfullerene *Nature* **318** 162–3
[2] Falcao E H L and Wudl F 2007 Carbon allotropes: beyond graphite and diamond *J. Chem. Technol. Biotechnol.* **82** 524–31
[3] Delgado J L, Herranz M A and Martin N 2008 The nano-forms of carbon *J. Mater. Chem.* **18** 1417–26
[4] Iijima S 1991 Helical microtubules of graphitic carbon *Nature* **354** 56–8
[5] Bethune D S, Klang C H, de Vries M S, Gorman G, Savoy R, Vazquez J and Beyers R 1993 Cobalt-catalysed growth of

carbon nanotubes with single-atomic-layer walls *Nature* **363** 605–7
[6] De Volder M F L, Tawfisk S H, Baughman R H and Hart A J 2013 Carbon nanotubes: present and future commercial applications *Science* **339** 535–9
[7] Novoselov K S, Geim A K, Morozov S V, Jiang D, Zhang Y, Dubonos S V, Grigorieva I V and Firsov A A 2004 Electric field effect in atomically thin carbon films *Science* **306** 666–9
[8] Geim A K and Novoselov K S 2007 The rise of graphene *Nat. Mater.* **6** 183–91
[9] Iijima S, Yudasaka M, Yamada R, Bandow S, Suenaga K, Kokai F and Takahashi K 1999 Nano-aggregates of single-walled graphitic carbon nano-horns *Chem. Phys. Lett.* **309** 165–70
[10] Zhu S and Xu G 2010 Single-walled carbon nanohorns and their applications *Nanoscale* **2** 2538–49
[11] Mochalin V N, Shenderova O, Ho D and Gogotsi Y 2012 The properties and applications of nanodiamonds *Nat. Nanotechnol.* **7** 11–23
[12] Ugarte D 1992 Curling and closure of graphitic networks under electron-beam irradiation *Nature* **359** 707–9
[13] Echegoyen L, Ortiz A, Chaur M N and Palkar A J 2010 Carbon nano onions *Chemistry of Nanocarbons* ed T Akasaka *et al* (Chichester: Wiley) pp 463–83
[14] Bartelmess J and Giordani S 2014 Carbon nano-onions (multi-layer fullerenes): chemistry and applications *Beilstein J. Nanotechnol.* **5** 1980–98
[15] Tran-Van A-F and Wegner H A 2014 Nano-rings with a handle—synthesis of substituted cycloparaphenylenes *Beilstein J. Nanotechnol.* **5** 1320–33
[16] Lewis S E 2015 Cycloparaphenylenes and related nanohoops *Chem. Soc. Rev.* **44** 2221–304
[17] Golder M R and Jasti R 2015 Syntheses of the smallest carbon nanohoops and the emergence of unique physical phenomena *Acc. Chem. Res.* **48** 557–66
[18] Tasis D, Tagmatarchis N, Bianco A and Prato M 2006 Chemistry of carbon nanotubes *Chem. Rev.* **106** 1105–36
[19] Singh P, Campidelli S, Giordani S, Bonifazi D, Bianco A and Prato M 2009 Organic functionalisation and characterisation of single-walled carbon nanotubes *Chem. Soc. Rev.* **38** 2214–30
[20] Zhao Y-L and Stoddart J F 2009 Noncovalent functionalization of single-walled carbon nanotubes *Acc. Chem. Res.* **42** 1161–71
[21] Allongue P, Delamar M, Desbat B, Fagebaume O, Hitmi R, Pinson J and Saveant J-M 1997 Covalent modification of carbon surfaces by aryl radicals generated from the electrochemical reduction of diazonium salts *J. Am. Chem. Soc.* **119** 201–7
[22] Bahr J L, Yang J, Kosynkin D V, Bronikowski M J, Smalley R E and Tour J M 2001 Functionalization of carbon nanotubes by electrochemical reduction of aryl diazonium salts: a bucky paper electrode *J. Am. Chem. Soc.* **123** 6536–42
[23] Bahr J L and Tour J M 2001 Highly functionalized carbon nanotubes using *in situ* generated diazonium compounds *Chem. Mater.* **13** 3823–4
[24] Flavin K, Lawrence K, Bartelmess J, Tasior M, Navio C, Bittencourt C, O'Shea D, Guldi D M and Giordani S 2011 Synthesis and characterization of novel boron azadipyrromethene single-walled carbon nanotube electron donor-acceptor conjugates *ACS Nano* **5** 1198–206
[25] Meinhardt T, Lang D, Dill H and Krueger A 2011 Pushing the functionality of diamond nanoparticles to new horizons: orthogonally functionalized nanodiamond using click chemistry *Adv. Funct. Mater.* **21** 494–500
[26] Ragoussi M-E, Casado S, Ribeiro-Viana R, de la Torre G, Rojo J and Torres T 2013 Selective carbohydrate–lectin interactions in covalent graphene- and SWCNT-based molecular recognition systems *Chem. Sci.* **4** 4035–41
[27] Ragoussi M-E, Katsukis G, Roth A, Malig J, de la Torre G, Guldi D M and Torres T 2014 Electron-donating behavior of few-layer graphene in covalent ensembles with electron-accepting phthalocyanines *J. Am. Chem. Soc.* **136** 4593–8
[28] Flavin K, Chaur M, Echegoyen L and Giordani S 2010 Functionalization of multilayer fullerenes (carbon nano-onions) using diazonium compounds and 'click' chemistry *Org. Lett.* **12** 840–3
[29] Feng, L, Wu, L and Qu X 2013 New horizons for diagnostics and therapeutic applications of graphene and graphene oxide *Adv. Mater.* **25** 168–86
[30] Yoo J M, Kang J H and Hong B H 2015 Graphene-based nanomaterials for versatile imaging studies *Chem. Soc. Rev.* **44** 4835–52
[31] Wu H-C, Chang X, Liu L, Zhao F and Zhao Y 2010 Chemistry of carbon nanotubes in biomedical applications *J. Mater. Chem.* **20** 1036–52
[32] Gong H, Peng R and Liu Z 2013 Carbon nanotubes for biomedical imaging: the recent advances *Adv. Drug Deliv. Rev.* **65** 1951–63
[33] Movia D, Prina Mello A, Bazou D, Volkov Y and Giordani S 2011 Integration of 3D cellular models in the toxicity screening of single-walled carbon nanotubes *ACS Nano* **5** 9278–90
[34] Perevedentseva E, Lin Y-C, Jani M and Cheng C-L 2013 Biomedical applications of nanodiamonds in imaging and therapy *Nanomedicine* **8** 2041–60
[35] Baptista F, Belhout S A, Giordani S and Quinn S J 2015 Recent developments in carbon nanomaterial sensors *Chem. Soc. Rev.* **44** 4433–53
[36] Bartelmess J, Quinn S J and Giordani S 2015 Carbon nanomaterials: multi-functional agents for biomedical fluorescence and Raman imaging *Chem. Soc. Rev.* **44** 4672–98
[37] Palkar A, Melin F, Cardona C M, Elliott B, Naskar A K, Edie D D Kumbhar A and Echegoyen L 2007 Reactivity differences between carbon nano onions (CNOs) prepared by different methods *Chem. Asian J.* **2** 625–33
[38] Keller N, Maksimova N I, Roddatis V V, Schur M, Mestl G, Butenko Y V, Kuznetsov V L and Schloegl R 2002 The catalytic use of onion-like carbon materials for styrene synthesis by oxidative dehydrogenation of ethylbenzene *Angew. Chem. Int. Edn. Engl.* **41** 1885–8
[39] Su D, Maksimova N I, Mestl G, Kuznetsov V L, Keller V Schloegl R and Keller N 2007 Oxidative dehydrogenation of ethylbenzene to styrene over ultra-dispersed diamond and onion-like carbon *Carbon* **45** 2145–51
[40] Yao Y, Wang X, Guo J, Yang X and Xu B 2008 Tribological property of onion-like fullerenes as lubricant additive *Mater. Lett.* **62** 2524–7
[41] Joly-Pottuz L, Vacher B, Ohmae N, Martin J M and Epicier T 2008 Anti-wear and friction reducing mechanisms of carbon nano-onions as lubricant additives *Tribol. Lett.* **30** 69–80
[42] Han F-D, Yao B and Bai Y-J 2011 Preparation of carbon nano-onions and their application as anode materials for rechargeable lithium-ion batteries *J. Phys. Chem.* C **115** 8923–7
[43] Wang Y, Han Z J, Yu S F, Song R R, Song H H, Ostrikov K and Yang H Y 2013 Core-leaf onion-like carbon/MnO_2 hybrid nano-urchins for rechargeable lithium-ion batteries *Carbon* **64** 230–6
[44] Pech D, Brunet M, Durou H, Huang P, Mochalin V, Gogotsi Y, Taberna P-L and Simon P 2010 Ultrahigh-power micrometre-sized supercapacitors based on onion-like carbon *Nat. Nanotechnol.* **5** 651–4
[45] McDonough J K, Frolov A I, Presser V, Niu J, Miller C H, Ubieto T, Fedorov M V and Gogotsi Y 2012 Influence of the structure of carbon onions on their electrochemical performance in supercapacitor electrodes *Carbon* **50** 3298–309
[46] Plonska-Brzezinska M E, Brus D M, Molina-Ontaria A and Echegoyen L 2013 Synthesis of carbon nano-onion and nickel hydroxide/oxide composites as supercapacitor electrodes *RSC Adv.* **3** 25891–901
[47] Macutkevic J *et al* 2008 Terahertz probing of onion-like carbon-PMMA composite films *Diamond Relat. Mater.* **17** 1608–12
[48] Yang M *et al* 2013 Functionalization of carbon nanoparticles modulates inflammatory cell recruitment and NLRP3 inflammasome activation *Small* **9** 4194–206
[49] Giordani S, Bartelmess J, Frasconi M, Biondi I, Cheung S, Grossi M, Wu D, Echegoyen L and O'Shea D F 2014 NIR fluorescence labelled carbon nano-onions: synthesis, analysis and cellular imaging *J. Mater. Chem.* B **2** 7459–63

[50] Bartelmess J et al 2014 Boron dipyrromethene (BODIPY) functionalized carbon nano-onions for high resolution cellular imaging *Nanoscale* **6** 13761–9
[51] Zhou L, Gao C, Zhu D, Xu W, Chen F F, Palkar A, Echegoyen L and Kong E S-W 2009 Facile functionalization of multilayer fullerenes (carbon nano-onions) by nitrene chemistry and 'grafting from' strategy *Chem. Eur. J.* **15** 1389–96
[52] Bartelmess J, Baldrighi M, Nardone V, Parisini E, Buck D, Echegoyen L and Giordani S 2015 Synthesis and characterization of far-red/NIR-fluorescent BODIPY dyes, solid-state fluorescence and application as fluorescent tags attached to carbon nano-onions *Chem. Eur. J.* **21** 9727–32
[53] Rettenbacher A S, Elliott B, Hudson J S, Amirkhanian A and Echegoyen L 2006 Preparation and functionalization of multilayer fullerenes (carbon nano-onions) *Chem. Eur. J.* **12** 376–87
[54] Palkar A, Kumbhar A, Athans A J and Echegoyen L 2008 Pyridyl-Functionalized and water-soluble carbon nano onions: first supramolecular complexes of carbon nano onions *Chem. Mater.* **20** 1685–7
[55] Luszczyn J, Plonska-Brzezinska M E, Palkar A, Dubis A T, Simionescu A, Simionescu D T, Kalska-Szostko B, Winkler K and Echegoyen L 2010 Small noncytotoxic carbon nano-onions: first covalent functionalization with biomolecules *Chem. Eur. J.* **16** 4870–80
[56] Plonska-Brzezinska M E, Mazurczyk J, Palys B, Breczko J, Lapinski A, Dubis A T and Echegoyen L 2012 Preparation and characterization of composites that contain small carbon nano-onions and conducting polyaniline *Chem. Eur. J.* **18** 2600–8
[57] Plonska-Brzezinska M E, Brus D M, Breczko J and Echegoyen L 2013 Carbon nano-onions and biocompatible polymers for flavonoid incorporation *Chem. Eur. J.* **19** 5019–24
[58] Sek S, Breczko J, Plonska-Brzezinska M E, Wilczewska A Z and Echegoyen L 2013 STM-Based molecular junction of carbon nano-onion *ChemPhysChem* **14** 96–100
[59] Nel A, Xia T, Maedler L and Li N 2006 Toxic potential of materials at the nanolevel *Science* **311** 622–7
[60] Berezin M Y and Achilefu S 2010 Fluorescence lifetime measurements and biological imaging *Chem. Rev.* **110** 2641–84
[61] Jokerst J V, Cole A J, Van de Sompel D, Gambhir S S, 2012 Gold nanorods for ovarian cancer detection with photoacoustic imaging and resection guidance via Raman imaging in living mice *ACS Nano* **6** 10366–77